Picosecond Holographic-Grating Spectroscopy

Duppen, K.

Published in:
Science

DOI:
10.1126/science.237.4819.1147

83. C. B. Officer and C. L. Drake, *Science* **227**, 1161 (1985).
84. V. Courtillot, J. Besse, D. Vandamme, J. J. Jaeger, R. Montigny, *C. R. Acad. Sci.* **303**, 863 (1986); V. Courtillot *et al.*, *Earth Planet. Sci. Lett.* **80**, 361 (1986).
85. V. Courtillot and S. Cisowski, *Eos* **68**, 193 (1987).
86. C. B. Officer *et al.*, *Nature (London)* **326**, 143 (1987).
87. R. W. Griffiths, *Earth Planet. Sci. Lett.* **78**, 435 (1986).
88. The Cretaceous-Tertiary and Permo-Triassic events discussed so far dominate the mass extinction records (*82*). It has been suggested that even smaller extinction events may be related to volcanism and plume activity [J. W. Morgan, *Eos* **67**, 391 (abstr.) (1986)]. The ongoing controversy regarding the reality of the 30-million-year "periodicity" in the reversal rate and extinctions is interesting in this respect (*36, 61*), although we will not discuss it further here.
89. W. Alvarez, *Eos* **67**, 649 (1986).
90. D. M. Raup, *The Nemesis Affair: A Story of the Death of Dinosaurs and the Ways of Science* (Norton, New York, 1986).
91. This article is dedicated to Allan Cox who introduced one of us (V.C.) and many others to the fascinating world of paleomagnetism and plate tectonics. The paper was written while V.C. enjoyed the friendly and stimulating atmosphere of the Department of Geological Sciences, University of California at Santa Barbara, which is thanked for partial support. Support for this research was also provided by Ministère de l'Education Nationale, Institut de Physique du Globe and Institut National des Sciences de l'Univers (Centre National de la Recherche Scientifique). Discussion with and comments from D. Anderson, M. Fuller, C. Jaupart, J. L. Le Mouël, R. Merrill, J. Morgan, J. P. Poirier, and F. Spera, who read a first version of this paper, are gratefully acknowledged. Also acknowledged is help in typing from P. Mori and E. Dzuro, and in drafting from D. Crouch and G. Dupin. The following contributed comments, reprints, or preprints at various stages: D. Anderson, T. Atwater, R. Clayton, A. Fabre, B. Hager, D. Jurdy, D. Loper, C. B. Officer, P. Patriat, J. P. Poirier, J. Ségoufin, and N. Sleep. This is Institut de Physique du Globe contribution NS 965.

Picosecond Holographic-Grating Spectroscopy

D. A. WIERSMA AND K. DUPPEN

Interfering light waves produce an optical interference pattern in any medium that interacts with light. This modulation of some physical parameter of the system acts as a classical holographic grating for optical radiation. When such a grating is produced through interaction of pulsed light waves with an optical transition, a transient grating is formed whose decay is a measure of the relaxation time of the excited state. Transient gratings can be formed in real space or in frequency space depending on the time ordering of the interfering light waves. The two gratings are related by a space-time transformation and contain complementary information on the optical dynamics of a system. The status of a grating can be probed by a delayed third pulse, which diffracts off this grating in a direction determined by the wave vector difference of the interfering light beams. This generalized concept of a transient grating can be used to interpret many picosecond-pulse optical experiments on condensed-phase systems. Examples of some low-temperature experiments will be presented. In principle, many of these experiments could also be performed by using stochastic broad-band excitation. In these nonlinear photon-interference experiments the time resolution is determined by the correlation time of the light source rather than its pulse width.

WITH RECENT ADVANCES IN DYE-LASER TECHNOLOGY, interest in the field of optical spectroscopy has shifted from spectral analysis to optical dynamics. Whereas Galileo Galilei used his heartbeat to time-resolve dynamics (*1*), physical processes can now be measured optically on a time scale where light travels only tens of micrometers. Optical pulses with a duration of a picosecond or less that can be tuned from the near ultraviolet to the near infrared are now readily available; visible pulses of only a few optical cycles have already been reported (*2*).

Fleming has recently reviewed the applications of picosecond spectroscopy in chemistry (*3*). In this article we highlight only a certain class of pulsed optical experiments; we concentrate on three-pulse optical pump-probe experiments in which the sample is excited with two interfering light pulses that produce a real-time hologram or transient grating. The decay of this transient grating is monitored by the use of a third time-delayed probe pulse that diffracts off this grating in a well-defined direction.

The type of transient grating formed depends on the time coincidence of the excitation pulses. In the case of time-coincident pulses a transient spatial grating is formed, which resembles a classical ruled or holographic grating. When the pulses are not coincident, a nonclassical holographic population grating in the frequency domain is generated. The fringe spacing in this "frequency" grating is $1/t_{12}$, where t_{12} is the time interval between the excitation pulses. Diffraction off this grating yields signals that are delayed by the same time interval t_{12}. These signals are called photon echoes.

The buildup of any grating is sensitive to the phase difference of the interfering light beams; the phase difference must be kept constant during the preparation period. Burland and co-workers (*4*) showed that the temporal buildup of a permanent spatial grating, formed by a photochemical reaction, contains information about the order, quantum yield, and spectroscopy of the intermediates of this reaction. Dynamical information about the optical pumping cycle of an optical transition is also contained in the buildup of the accumulated frequency-domain grating (*5*), but no experiments have as yet exploited this possibility.

The decay of a transient spatial grating is generally caused by population-relaxation and spatial-diffusion processes. These processes are known as T_1-type processes in optical dynamics. They often proceed at room temperature on a picosecond or even nanosecond time scale so that experiments with transient spatial gratings are feasible over a large temperature range. This field has been reviewed by Eichler (*6*) and more recently by Fayer (*7*). Scattering experi-

The authors are at the Department of Physical Chemistry, Nijenborgh 16, 9747 AG, and at the Department of Solid State Physics, Melleweg 1, 9718 EP, Groningen, the Netherlands.

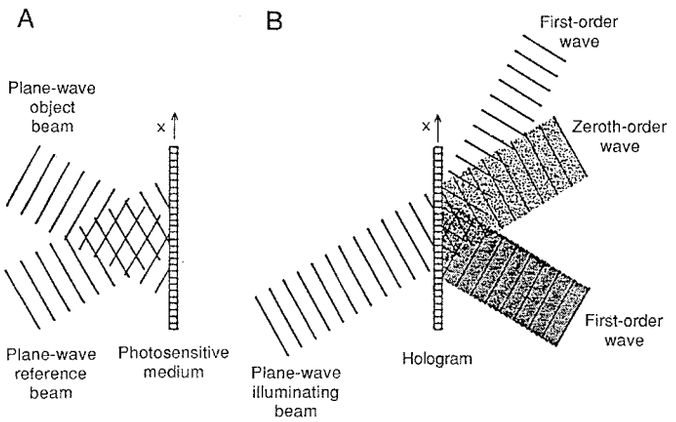

Fig. 1. (**A**) Formation and (**B**) read-out of a plane hologram. For thicker holograms only the first-order reconstructed (diffracted) wave (that points downward in the figure) would survive.

ments with frequency-domain gratings are better known as (stimulated) photon-echo experiments. The frequency-domain population grating not only decays through population relaxation and spatial diffusion but also by optical dephasing and spectral diffusion, which can be characterized by a relaxation constant designated T_2. Optical dephasing is often a rapid process except at lower temperatures. Thus photon-echo experiments are only feasible on samples cooled to low temperature.

Historically, a photon echo (*8*) has been considered the optical analog of the spin echo (*9*) and its formation is usually described in what is known as the "rotating frame picture." Reviews by Hartmann (*10*) and Brewer and Hahn (*11*) of photon-echo research present in vivid detail this pictorial and powerful approach toward understanding the echo phenomenon. We will describe these multiple optical pulse effects in terms of scattering from a transient grating (*12*) and show that with this approach, which unifies photon echoes with transient holographic-grating scattering, many seemingly complex optical pulse effects are easily understood.

Holography and Diffraction

Modern dynamical optical spectroscopy is in many ways related to holography. In holography (*13*), the phase and amplitude of light waves reflected from an object can be stored in a photosensitive medium by interference of these waves with a reference beam. The optical image can be reconstructed by illumination of the developed hologram. The most simple hologram is formed by letting two plane waves, one called the object beam and the other the reference beam, interfere at an angle 2θ in a photosensitive medium (Fig. 1A). The waves can be described by functions of the form:

$$\mathbf{E}(\mathbf{r},\omega,t) = \mathbf{E}_0(\mathbf{r},t)\exp[-i(\omega t - \mathbf{k}\cdot\mathbf{r} + \Phi)] \quad (1)$$

where the electric field amplitude $\mathbf{E}$ of the light is written as an envelope $\mathbf{E}_0$, which varies relatively slowly in space $\mathbf{r}$ and time t, and a rapidly varying part, which contains the optical frequency ω, the momentum $\mathbf{k}$, and an additional phase factor Φ. When two of these beams are crossed (Fig. 1A), the interference pattern in the x-direction has the form:

$$I(x) = 2I[1 + \cos(\frac{2\pi}{\Lambda}x + \Phi_{12})] \quad (2)$$

Here I is the intensity in each beam, Φ_{12} is the phase difference between the two beams, and Λ is the fringe spacing, which is given by

$$\Lambda = \lambda/(2\sin\theta) \quad (3)$$

where λ is the wavelength of the interacting beams. Note that the interference pattern contains information on the phase difference between the object and reference beam, which explains the necessity of a stable optical setup for making a hologram. The planes perpendicular to the x-axis and spaced by the fringe spacing are called the Bragg planes. When such a hologram is illuminated by the reference beam only (Fig. 1B), reconstruction of the object beam occurs (a diffraction phenomenon). Two first-order waves emerge at an angle 2θ to the zeroth-order wave from the hologram. The wave that proceeds in the same direction as the original object beam has the identical phase as this beam, whereas the other wave is the phase conjugate to the original beam.

For a thick hologram the Bragg condition for the reference beam must also be fulfilled, so that only one diffracted beam has appreciable intensity. The direction of this beam is given by reflection of the reference beam at the grating planes. On reversing the direction of this illuminating beam, the only diffracted wave formed is a wave conjugate to the original object beam. Thus optical phase conjugation (*14*) can be considered a form of dynamic holography.

We have assumed so far that the frequencies of the interfering light waves are identical. When they are of different frequencies, ω_1 and ω_2, a grating is formed that propagates at the frequency difference $\Omega = \omega_1 - \omega_2$. Optical waves that are scattered from this moving grating pick up this frequency difference, which gives rise to scattered waves of frequencies $2\omega_1 - \omega_2$ and $2\omega_2 - \omega_1$. These processes are usually classified as four-wave mixing effects and are calculated in terms of the optical nonlinear susceptibility of the material. The connection between these two-color scattering effects and holographic-grating scattering has already been recognized by Eichler (*15*).

The probe pulse can also be of a different color than the two excitation pulses. The decay of a spatial grating is often studied by this pump-probe scheme to prevent the problem of stray light from the excitation pulses. In the case of a frequency-domain grating, a new photon-echo effect occurs: the two-color photon echo (*16*). Depending on the time ordering and color of the excitation and probe pulses, one can thus measure a transient spatial grating, a

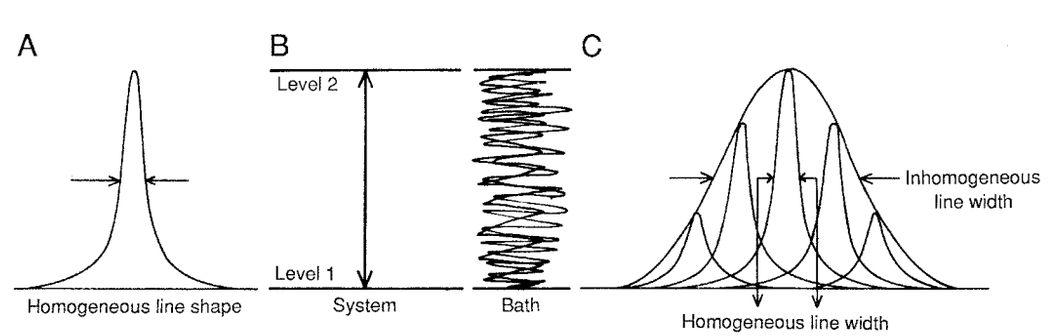

Fig. 2. (**A**) Lorentzian line shape of a damped oscillator with a width of $\Gamma_0/(2\pi)$ or a homogeneous line shape of a two-level system with a width of $(\pi T_2)^{-1}$. (**B**) The homogeneous width of a two-level system is due to interaction with a thermal bath. (**C**) The Gaussian line shape that is often observed is caused by inhomogeneity of the sample.

four-wave mixing effect, or a two-color photon echo. These aspects will be dealt with below after a short discussion of some optical properties of dynamical systems.

Population Relaxation and Optical Dephasing: T_1 and T_2

In all transient-grating experiments, decays are measured which are interpreted according to certain models. Relaxation is characterized as either population relaxation (T_1) or optical dephasing (T_2). The former process involves transfer of population from the excited state to a lower state, either radiatively or by a radiationless process, until thermodynamic equilibrium is reached. If this would be the only relaxation process and the sample were perfect, the line shape of the optical transition would be Lorentzian (Fig. 2A) with a full width at half maximum (FWHM) of $(2\pi T_1)^{-1}$ (rad sec^{-1}). This is called the homogeneous line width, which is basically due to coupling of the optical excitation with some kind of background that is at thermal equilibrium (Fig. 2B). In practice this Lorentzian is often buried beneath a Gaussian-shaped line (Fig. 2C). This Gaussian broadening of the absorption line is often caused by imperfections in the sample. The width of this distribution is called the inhomogeneous width. Unless the excited state lifetime is extremely short, the inhomogeneous width far exceeds the homogeneous width. This is true even in samples cooled to liquid helium temperature, for which absorption lines are the sharpest.

Next to these population relaxation processes, pure dephasing processes (T_2^*) occur that leave the populations of the states intact but perturb the frequency of the optical transition. These processes affect the homogeneous width of an optical transition as well, so that the total homogeneous width (FWHM) becomes $(\pi T_2)^{-1}$ (rad sec^{-1}), whereby

$$1/T_2 = 1/T_2^* + 1/2T_1 \quad (4)$$

This relation shows that if pure dephasing processes are negligible, then the relation $T_2 = 2T_1$ holds. Since the homogeneous width induced by both T_1 and T_2^* processes is generally obscured by inhomogeneous broadening, time-domain experiments are needed to provide information on the optical dynamics of the system. The transient spatial grating decays with the population relaxation time T_1, whereas the frequency-domain grating decays with either time T_2 or T_1 depending on whether the self-diffracted or the probe pulse–induced scattered signal is studied.

Technology of Transient-Grating Scattering Spectroscopy

To achieve the necessary flexibility in performing a variety of transient-grating experiments, a dual picosecond dye-laser system is needed. A typical setup that we have used is shown in Fig. 3A. A mode-locked argon-ion laser is used that produces 100-psec pulses at an 82-MHz repetition rate. This laser synchronously pumps two dye lasers (*17*) that produce pulses as short as a few picoseconds and are independently tunable from ~530 nm to ~1000 nm. These pulses are then amplified in two stages to the microjoule level by a neodymium-YAG (yttrium-aluminum-garnet) laser that operates at 10 Hz. The time resolution in these two-color pulsed experiments is about 10 psec, which is determined mainly by the timing jitter between the pulses of the two dye lasers. There are several points to note here. First, a mode-locked YAG laser can be used instead of an argon-ion laser to pump the dye lasers. In that case, the timing jitter between the pulses is reduced somewhat (*18*). More importantly, the pulses of the YAG laser can be compressed to a few picoseconds (*19*), which allows the generation of dye laser pulses of a few hundred femtoseconds by synchronous pumping (*20*). The timing jitter between pulses from the two dye lasers is then expected to be less than 1 psec. Second, a copper-vapor laser may be used to amplify the picosecond dye lasers at a repetition rate of a few kilohertz (*21*). When a YAG laser is used as the synchronous pump, a regenerative amplifier at a 1-kHz repetition rate may be used for the same purpose (*22*); signal averaging is obviously more efficient at a few kilohertz than at 10 Hz.

The amplified dye-laser pulses are split, delayed, and recombined in a fashion that depends on the experiment. The signal beam, generated in the coherent pump-probe process, is spatially isolated and spectrally resolved by a monochromator and detected by a photomultiplier. The photocurrent from the photomultiplier is processed by a boxcar analyzer, which is a signal amplifier and averager that has a time gate that coincides with the photomultiplier signal. The output is displayed on an x-y recorder with an x-axis output that is proportional to the time delay of the probe pulse. A typical layout for multiple pulse (two-color) optical experiments is shown in Fig. 3B. The signal that scatters from a spatial grating is time coincident with the probe pulse. In nanosecond photon-echo experiments, it is possible to use a fast optical shutter to discriminate against the stray light of the excitation and probe pulses. For picosecond photon-echo detection we have used the technique of up-conversion as an optical gate (*23*), whereby the echo is mixed with a synchronized amplified probe pulse of different frequency in an optical nonlinear crystal such as ADP (ammonium dihydrophosphate).

Transient Spatial Gratings

When two parallel-polarized time-coincident light beams cross in a medium, the optical interference pattern causes a spatially periodic change of the physical properties of the system. In a macroscopic description of the system this change can be expressed in terms of the spatial modulation of the complex index of refraction $\eta = n + i\kappa$. The optical interference pattern leads to two types of gratings: a phase grating from the spatial modulation of n, and a volume grating from the absorptive part κ of η. These two gratings are connected by a Kramers-Kronig relation that results from causality. To make an explicit connection between the macroscopic properties of these spatial gratings and the underlying microscopic dynamics, a model for the system under study is needed. The most simple model consists of a two-level system coupled to a heat bath (Fig. 2B). An example is a guest molecule with a ground state and an electronically excited state that is embedded in a lattice. Such a system can conveniently be described by a damped harmonic oscillator, for which the dispersion of η is given by (*24*):

$$\eta^2 - 1 = Nf'/(\omega_0^2 - \omega^2 - i\omega\Gamma_0) \quad (5)$$

Here N is the number density of molecules in the ground state; $f' = 4\pi e^2 f/m$ where f, m, and e are the oscillator strength and the electronic mass and charge, respectively; and ω_0 and Γ_0 are the central absorption frequency and line width of the transition. Note that the damping in this model only results from population-relaxation processes.

Using this model Nelson *et al.* (*25*) have shown that the diffraction efficiency for an excited state grating $[n_{ex}(\omega)]$ takes the following simple form:

$$n_{ex}(\omega) = P_c\, k_0(\omega_0)\, k_0(\omega) \quad (6)$$

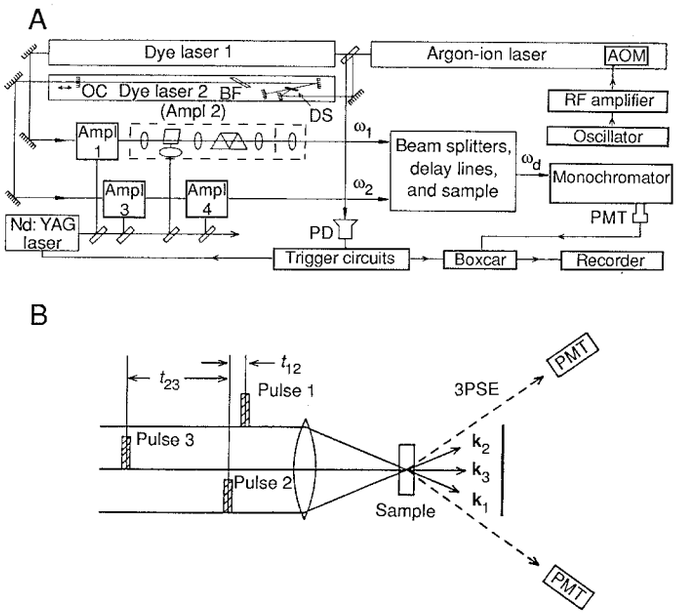

Fig. 3. (**A**) Experimental apparatus used for multiple-pulse optical transient-grating studies. Abbreviations: AOM, acousto-optic modulator; RF, radio frequency; BF, birefringent filter; DS, dye sheet; OC, output coupler; Ampl, amplifier; PMT, photomultiplier; PD, photodiode. The detected frequency is ω_d. (**B**) Layout for picosecond transient-grating experiments. All pulses make angles of a few degrees with one another and usually lie in one plane. If pulses 1 and 2 create a thin spatial grating, then the probe pulse scatters symmetrically into the directions $\mathbf{k}_2 - \mathbf{k}_1 \pm \mathbf{k}_3$; if a frequency-domain grating is generated, then because of causality the scattered signal (photon echo) is only generated along the direction given by the vector $\mathbf{k}_2 - \mathbf{k}_1 + \mathbf{k}_3$.

Here P_c is a proportionality constant that contains parameters of the system such as the optical density, the thickness of the sample, and the fraction of molecules excited. The functions $k_0(\omega_0)$ and $k_0(\omega)$ are defined as follows:

$$k_0(\omega_0) = (1/2n_0)\ (N_0 f'/\Gamma_0\omega_0) \quad (7)$$

$$k_0(\omega) = k_0(\omega_0)\ (\Gamma_0/2)^2/[(\omega - \omega_0)^2 + (\Gamma_0/2)^2] \quad (8)$$

where N_0 is the number density of guest molecules in the unperturbed sample and n_0 is the number of molecules affected by the excitation process.

Examination of Eqs. 6 through 8 shows that the dispersion of the diffraction efficiency due to the combined effect of a phase and volume grating for resonance excitation of the damped oscillator is simply given by a Lorentzian of width $\Gamma_0/(2\pi)$. The decay of the spatial grating is thus predicted to be exponential with a rate constant of $2\Gamma_0$. This important result is also valid when the line shape of the transition under study is not Lorentzian (Fig. 2A) but Gaussian as a result of inhomogeneous broadening (Fig. 2C). The identical result is obtained (*12*) from a quantum mechanical calculation of a two-level system: in a spatial-grating scattering experiment one can only obtain information on population-relaxation processes (T_1) and not on dephasing (T_2) processes.

Many spatial-grating scattering experiments have been performed on optical transitions of molecules and atoms in the condensed phase and have recently been reviewed (*7*). We will discuss a few examples and start with a transient-grating experiment that involves a vibrationally excited transition (*26*). In the level scheme shown in Fig. 4A, levels a and c represent the ground and electronically excited state of the pentacene guest molecule embedded in a naphthalene host, whereas levels b and d are the corresponding vibrational levels of these states. The transient spatial grating is

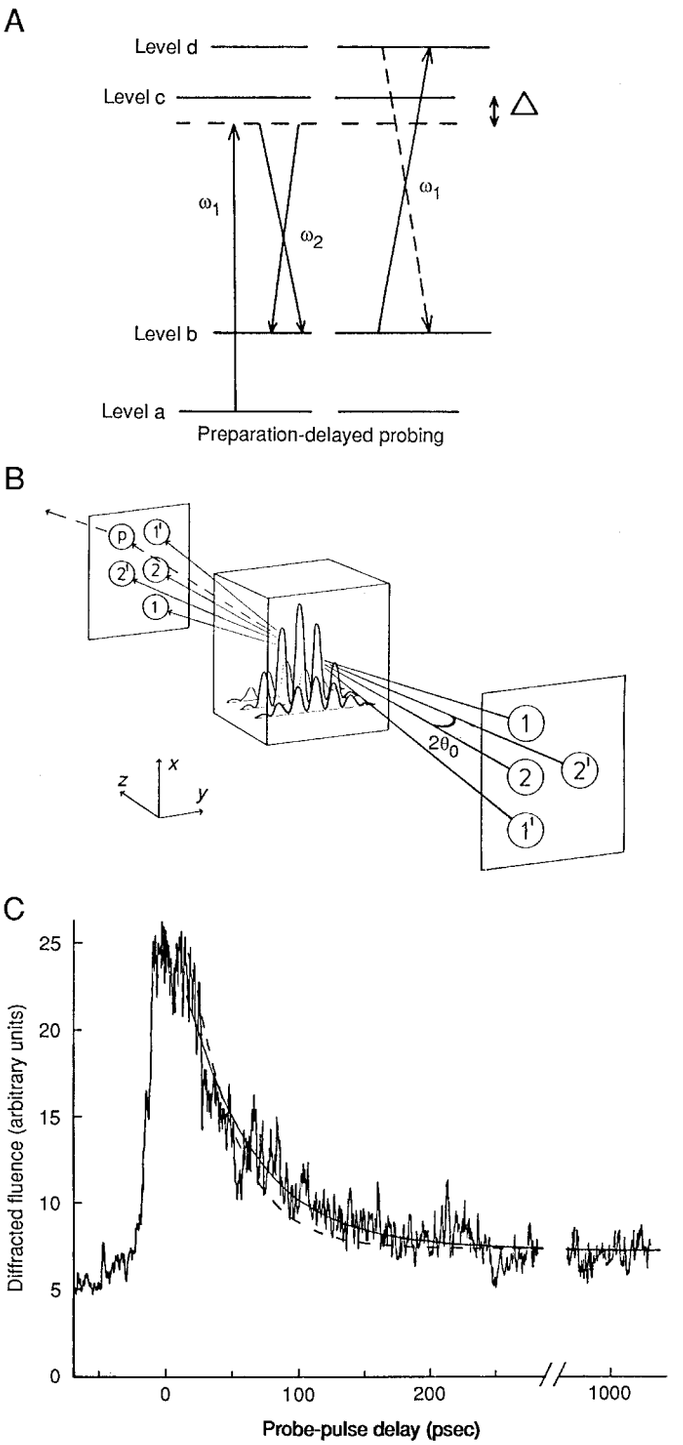

Fig. 4. Schematics and results of a scattering experiment involving a transient vibrational grating. (**A**) The relevant level scheme and the excitation and probing processes. Multiple (near) resonances are used to study the dilute guest molecules (10 ppm of pentacene) in the host crystal (naphthalene). The crossed beams in the preparation stage are off-resonance by a frequency Δ and produce the vibrational grating at ω_{ba}. The probe process is fully resonant. (**B**) Schematic of the actual beam geometries used in the experiment and the vibrational volume grating created in the sample. Beams 1, 2, and 2′ are time-coincident, while beam 1′ is delayed. (**C**) A typical result for pentacene in naphthalene, cooled to 1.5 K. The solid line presents the fit discussed in the text.

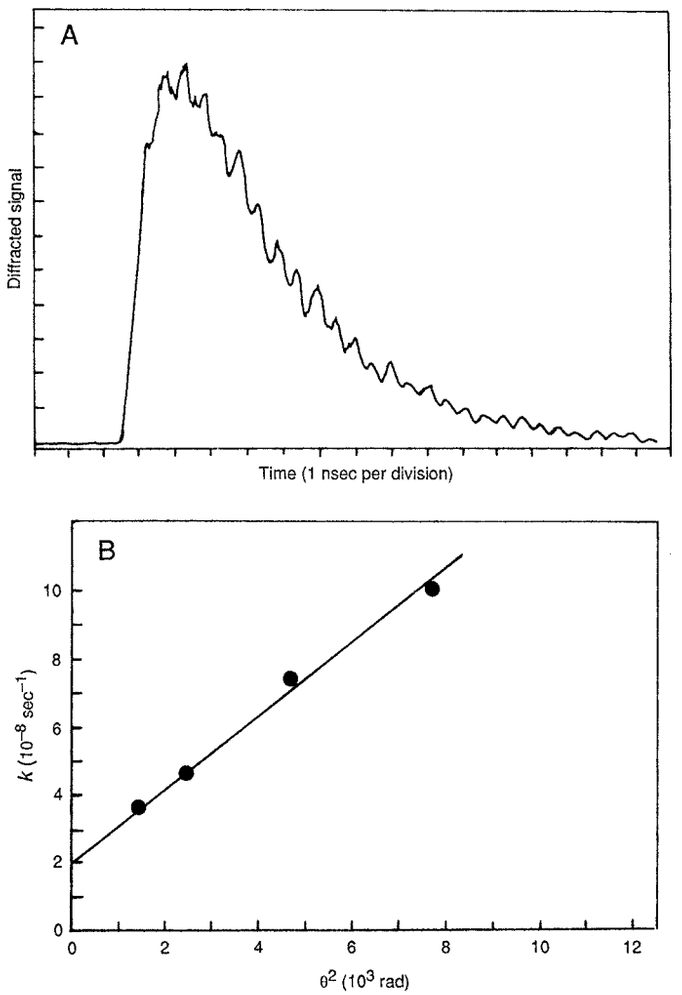

Fig. 5. (**A**) Transient exciton-grating scattering in crystalline anthracene with a fringe spacing of 9.6 μm at a temperature of 10 K. The grating decay time of T = 3.2 nsec is caused both by the lifetime of the exciton and by spatial diffusion of excitation. The "ripples" in the decay are due to interference with phonons scattered back from the surfaces of the sample. (**B**) Plot of observed grating-decay rate constant $k = T^{-1}$ as a function of the angle between the grating-forming beams. From this experiment it can be deduced that the diffusion constant of excitons in anthracene is D = 1.8 cm^2/sec at this temperature. [Reproduced with permission from Elsevier Science Press (*31*)]

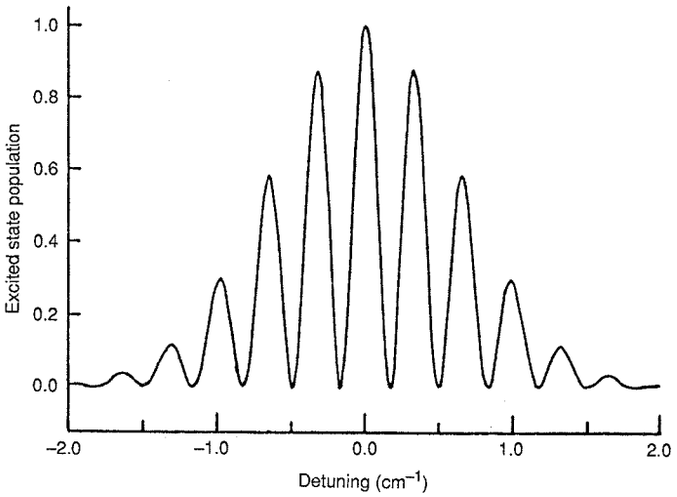

Fig. 6. Frequency-domain grating as formed in the excited state by two resonant short pulses separated by 100 psec. The horizontal axis gives the position in the inhomogeneous line (the detuning). The Gaussian envelope of the modulation represents a width of 1.5 cm^{-1}; it is assumed that $T_2 >>$ 100 psec.

prepared on the vibrational transition at 756 cm^{-1} in the electronic ground state by the interference of two resonant two-photon excitation processes. This rather complicated excitation process involves three time-coincident beams of two different colors. A fourth beam is employed to probe the dynamics of the prepared vibrational population distribution (Fig. 4B). The solid line in Fig. 4C presents an exponential fit to the measured decay with T_1 lifetime constants of 33 psec for level d [independently known from photon-echo experiments (*27*)] and 51 psec for level b. This latter number is in agreement with the results that had been obtained previously in a time-resolved coherent anti-Stokes scattering (CARS) experiment in which the dephasing time T_2 was measured (*28*). Thus, for the sample at low temperature, $T_2 = 2T_1$ for this vibrational transition. Despite the complexity of this type of experiment, it seems to be the most promising approach for measuring vibrational population relaxation times on the ground state potential energy surface. In terms of nonlinear optics, this vibrational-grating scattering experiment falls in the category of six-wave mixing.

We have assumed so far that the optical excitation is spatially stationary. If diffusion of the excitation occurs, then the transient grating will be erased as well. The effect of excitation diffusion on the measured decay of the spatial grating depends on the fringe spacing. In the presence of excitation diffusion the decay time T of the diffracted light is given by (*29*):

$$1/T = 1/T_1 + (4\pi^2/\Lambda^2)D \qquad (9)$$

where T_1 is the excited state lifetime, Λ is the fringe spacing, and D is the diffusion constant. This expression shows that a measurement of T as a function of the fringe spacing leads to an independent determination of T_1 and D. Spatial diffusion effects are expected to occur in excitonic systems such as semiconductors and molecular solids. The first transient-grating experiment on mobile excitons was performed by Aoyagi *et al.* (*30*) on CuCl. A similar measurement on the molecular solid anthracene was recently performed by Fayer and co-workers (*31*). A typical result and a plot of the measured grating decay versus fringe spacing are shown in Fig. 5. It appears that the diffusion constant of excitons in anthracene at 10 K is an order of magnitude less than for excitons in CuCl. The excitonic motion in anthracene can only be coherent (wavelike) on a distance scale that is less than the fringe spacing that was used.

A few additional comments about transient spatial gratings should be made. First, a third type of spatial grating, the acoustic grating, also exists. When part of the photonic energy is converted into heat by some kind of relaxation process, counterpropagating ultrasonic waves (phonons) are launched whose wavelength and spatial direction match the optical interference pattern. The effect of scattering from this ultrasonic-wave grating manifests itself as "ripples" on the decay [see (*7*) and (*25*)]. Second, all the gratings discussed above involve a spatial modulation of a physical parameter of the material and are called concentration gratings. To induce this type of grating, the polarization of the grating-forming beams must be nonorthogonal. If the polarizations of the grating-forming beams are orthogonal and remain so in the sample (isotropic or uniaxial system), an orientation or polarization grating (*32*) is formed. This type of grating can be generated in liquids and semiconductors. In liquids or liquid crystals the study of a polarization grating circumvents the problem of interference with an acoustic-wave grating (*33*). The polarization grating also holds great promise for the study of momentum relaxation in semiconductors. Initial measurements

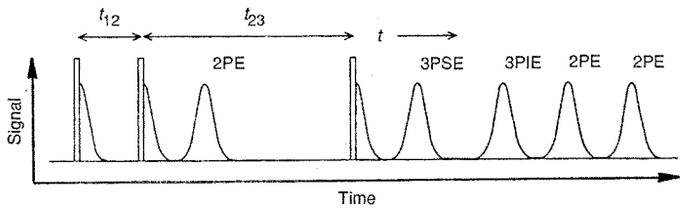

Fig. 7. Pulse sequence and observed photon echoes in a scattering experiment that involves three-pulse transient frequency-domain gratings. The decays immediately following the excitation pulses are free-induction decays. Abbreviations: 2PE, two-pulse photon echo; 3PSE, three-pulse stimulated photon echo; 3PIE, three-pulse image photon echo.

on germanium show that the relaxation time for hole momentum is less than 1 psec (*34*).

Transient Frequency-Domain Gratings

When one of the interfering light beams that produce the grating (Fig. 1A) is delayed with respect to the other beam, instead of a spatial grating a frequency-domain grating is formed. To understand this transition from space into the frequency-domain, a quantum mechanical instead of a classical calculation needs to be performed (*12*). After application of two resonant pulses that are separated by time t_{12} on the two-level system of Fig. 2B, the following results are obtained for the population distributions in the ground state (ρ_{11}) and excited state (ρ_{22}) at time t_{12}^{+} just after the second pulse:

$$\rho_{11}(t_{12}^{+}) = 1/2\{1 + \cos\theta_2[1 + (\cos\theta_1 - 1)e^{-t_{12}/T_1}] - \sin\theta_1 \sin\theta_2 \exp(-t_{12}/T_2)\cos(t_{12}\Delta - k_{12}x + \Phi_{12})\} \quad (10)$$

$$\rho_{22}(t_{12}^{+}) = 1 - \rho_{11}(t_{12}^{+}) \quad (11)$$

Here T_1 and T_2 are the constants that define the optical dynamics of the system, Δ (rad sec^{-1}) is the detuning from the center of the inhomogeneous line (Fig. 2C), k_{12} is $k_1 - k_2$, and θ_1 and θ_2 are the pulse angles of the first and second pulse, which are defined by

$$\theta = (\mu_{12}/\hbar) \cdot \int E_0(r,t)dt \quad (12)$$

where μ_{12} is the transition moment, $\hbar$ is Planck's constant, and $E_0(r,t)$ is the laser field strength.

For our purposes the most relevant term in ρ_{11} is the last one, which describes the grating that we are interested in. The result is in fact identical to the one derived for the spatial grating (Eq. 2) when t_{12} is taken to be zero, since $k_{12} = k_1 - k_2 = 2\pi/\Lambda$. In the more general situation where t_{12} is finite, the spatial grating is erased by a space-frequency transformation, which then gives a population distribution that is modulated in the frequency domain with a spatially modulated phase factor. A plot of the excited state grating is shown in Fig. 6 for maximum modulation depth ($\theta_1 = \theta_2 = \pi/2$) and a separation between the pulses of 100 psec. We assumed that the line shape of the transition is a Gaussian that results from inhomogeneities in the sample. Note that according to Eqs. 10 and 11 the amplitude of the grating decays exponentially with T_2 for the time delay between the excitation pulses. In analogy with a spatial grating, a third probe pulse will scatter off this grating under phase-matched conditions. Furthermore, because the fringe spacing in the frequency-domain grating is the inverse of the time interval between the excitation pulses, the diffracted signal is expected to be time-delayed by exactly this time interval. This time-delayed signal is known as the three-photon stimulated echo (3PSE), and its intensity depends both on T_2 (in the time interval t_{12}) and on T_1 (in the time interval t_{23}). In principle, the gratings can also decay by spectral diffusion. This is the frequency-domain analog of spatial diffusion. Although these effects are often related, they are certainly not identical.

In an actual three-pulse experiment many more photon echoes appear (Fig. 7). We want to discuss briefly now whether the frequency-grating picture can account for all these signals. First, all signals designated by 2PE are two-pulse photon echoes that result from the various two-pulse combinations in the sequence. In the grating picture these echoes must be considered as signals due to self-diffraction of the second pulse in a two-pulse sequence. The intensity of these signals as a function of the pulse separation decreases exponentially with the optical dephasing constant T_2. The occurrence of the 3PSE has been explained above as a time-delayed version of spatial-grating scattering, so only the three-pulse image echo (3PIE) remains to be explained. This echo occurs as a higher order scattering effect due to "cross talk" between a grating formed between the first two excitation pulses and a grating formed by the second and third pulses. Because this echo contains the same information as the 2PE, it has not been extensively studied in the optical domain.

We will now present a few examples of where the grating concept provides useful insight in the observed photon-echo phenomenon. The first 3PSE experiment we discuss concerns the radical triphenylmethyl doped into triphenylamine (*35*). The presence of a free electron spin on the radical that interacts with all the hydrogen atoms of the phenyl rings causes many (65,536) near-degenerate hyperfine levels in the ground and excited states. Since many of these

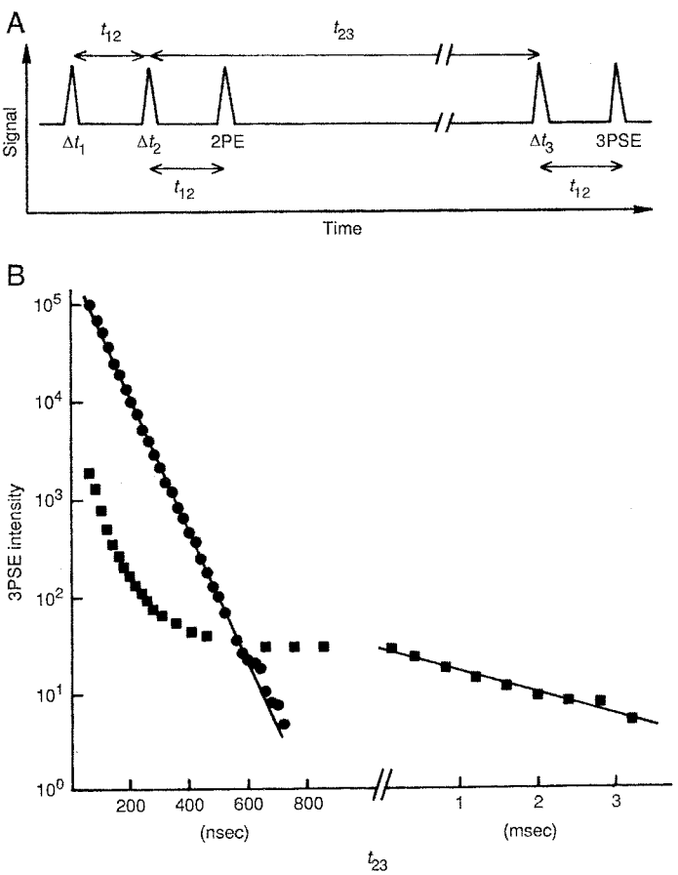

Fig. 8. (**A**) Pulse sequence and (**B**) results of a three-pulse photon echo experiment (3PSE) on the energetically lowest optical transition of triphenylmethyl doped into triphenylamine at 1.5 K with a magnetic field of 1.5 T (●) and without a magnetic field (■).

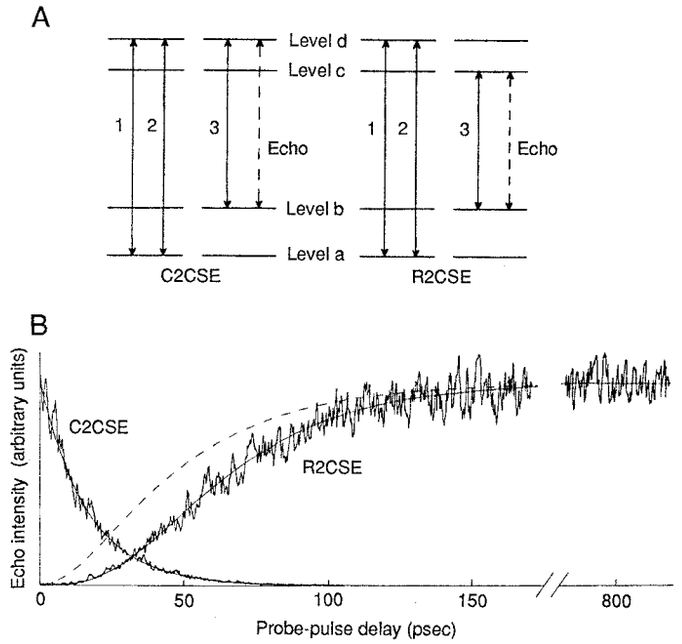

Fig. 9. (**A**) Level scheme and excitation and probing processes for two different types of two-color frequency-domain grating scattering effects (photon echoes), that is, the C2CSE (connected two-color stimulated echo) and the R2CSE (relaxed two-color stimulated echo). In these schemes time is increasing from left to right. The time separation between pulses 1 and 2 is 60 psec in both cases. The break in the center of the two level schemes indicates a variable delay for the probe pulse. (**B**) Experimentally observed echo intensities for both the C2CSE and the R2CSE. The dashed line is the predicted rise of the R2CSE intensity when direct relaxation would occur from level d to level c. The solid line was calculated by assuming a bottleneck in the vibrational relaxation dynamics.

levels can be excited in a pulsed optical experiment, the system cannot necessarily be described by a two-level system. Interestingly, a 3PSE was observed on a time scale much longer than the excited-state lifetime of the radical, which is only 130 nsec (Fig. 8). However, this echo disappeared in the presence of a magnetic field of a few tesla. To explain this phenomenon we first consider the situation in the presence of the magnetic field. The electron spin is quantized along the magnetic field, and the nuclear spin is quantized along the field direction of the electron, which means that the states can be characterized by quantum numbers m_S and m_I for the electron and nuclear spin, respectively. The optical selection rules are $\Delta m_S = \Delta m_I = 0$ and the system is effectively a two-level system. The hyperfine levels in a high magnetic field appear to the radiation field just as a kind of inhomogeneity. Thus the decay of the 3PSE is determined by the fluorescence lifetime T_1 (Fig. 8). In the absence of a magnetic field, optical branching occurs, which means that each level in the ground state is optically connected to many levels in the excited state and vice versa. The multilevel nature of the optical transition gives rise to a frequency-domain population grating in the levels optically connected, which automatically leads to a grating in the population distribution of spin levels. When these population distributions are probed, the grating at the optical transition will decay on a time scale determined by the lifetime of the radical. However, the spin grating, which is transformed into an optical grating by the probe pulse, has a lifetime determined by spin relaxation, which can be very long compared to the fluorescence lifetime. A similar effect occurs in the inorganic system of praseodymium ions in a lanthanum fluoride single crystal (Pr^{3+}/LaF_3); here photon echoes were observed (*36*) even after a probe-pulse delay as long as 30 minutes. Thus these systems act as optical memories (*37*) with the information stored in spin states.

The second example involves stimulated photon-echo experiments on pentacene in naphthalene. The relevant level structure and pulse sequence are shown in Fig. 9A. In both experiments discussed below the transient frequency-domain grating is generated on the vibronic transition between levels a and d. The probing of this grating is now done with a pulse of a different color. The first two excitation pulses generate a frequency-domain population grating in both the ground and excited state, in this case levels a and d. A photon echo can be generated on the transition from ⟨d| to |b⟩ because in one of the states a frequency-domain grating is present. The decay of this grating will proceed with the vibration relaxation time of level d. This is known as the connected two-color stimulated photon echo (C2CSE), which smoothly transforms into a tri-transition echo when the third pulse is applied before the second pulse (*16*). The situation is even more interesting when the probe pulse connects states c and b, since neither level is populated initially. However, through vibrational relaxation, population from level d will populate level c. Thus a population grating initially present in level d will relax into level c. A probe pulse at the transition between ⟨c| and |b⟩ will then be able to scatter from this relaxed grating. This is the relaxed two-color stimulated echo (R2CSE) (*38*). The decay of the C2CSE and the rise of the R2CSE as a function of the delay of the probe pulse are shown in Fig. 9B. The dotted line is the predicted rise of the R2CSE in case level d relaxes directly into level c. The discrepancy with the experimental result indicates that between d and c there must be at least one other level that acts as a bottleneck in the relaxation process from d to c. Thus these two-color experiments are useful probes of the dynamics of vibrational relaxation.

Stochastic Light Fields

Transient-grating spectroscopy is usually performed with pulsed excitation. The achievable time resolution is determined by the pulse width of the exciting laser. However, many forms of grating spectroscopy can also be performed with stochastic broad-band excitation (*39*). In these experiments it is the correlation time of the exciting radiation that determines the time resolution. Since the correlation time can be viewed as a pseudopulse, one can use the transient grating picture to predict all the interference phenomena. For a chaotic light source that obeys Gaussian photon statistics, the correlation time τ of the light source is related to its spectral bandwidth $\Delta\lambda$ by the relation (*40*)

$$\tau_c = \lambda_0^2/(\pi c \Delta\lambda) \qquad (13)$$

where λ_0 is the central frequency of the light source and c is the speed of light. Many organic dyes can be made to lase over a bandwidth of about 8 nm in the visible spectrum, which allows a time resolution of about 50 fsec. Moreover, these stochastic photon-interference experiments can be done with an extremely simple apparatus; in many cases only a nitrogen pumped dye-laser system and some standard spectroscopic equipment are needed. The impact of nonlinear photon-interference spectroscopy on the field of transient-grating and more generally on four-wave mixing spectroscopy is already significant and continues to grow. It certainly presents a challenge to those who insist on using pulsed radiation in their spectroscopic experiments.

REFERENCES AND NOTES

1. G. Galilei, *Discorsi e Dimostrazioni Matematichi intorno a due nuove Science* (Elsevier, Leiden, 1638) [H. Crew and A. de Salvio, Transl. (Northwestern Univ. Press, Evanston, IL, 1950)].
2. C. H. Brito-Cruz, R. L. Fork, C. V. Shank; paper presented at the Conference on Lasers and Electro-Optics (CLEO), Lasers and Electro-Optics Society and Optical

Society of America, Baltimore, MD, 27 April to 1 May 1987.
3. G. R. Fleming: *Chemical Applications of Ultrafast Spectroscopy, International Series of Monographs on Chemistry Number 13* (Clarendon, Oxford, 1986).
4. G. C. Bjorkland, D. M. Burland, D. C. Alvarez, *J. Chem. Phys.* **73**, 4321 (1980); D. M. Burland, *Acc. Chem. Res.* **16**, 218 (1983).
5. W. H. Hesselink and D. A. Wiersma, *Phys. Rev. Lett.* **43**, 1991 (1979).
6. H. J. Eichler, *Opt. Acta* **24**, 631 (1977).
7. M. D. Fayer, *Annu. Rev. Phys. Chem.* **33**, 63 (1982).
8. N. A. Kurnit, I. D. Abella, S. R. Hartmann, *Phys. Rev. Lett.* **13**, 567 (1964).
9. E. L. Hahn, *Phys. Rev.* **80**, 580 (1950).
10. S. R. Hartmann, *Sci. Am.* **218**, 32 (April 1968).
11. R. G. Brewer and E. L. Hahn, *ibid.* **251**, 42 (December 1984).
12. K. Duppen and D. A. Wiersma, *J. Opt. Soc. Am. B* **3**, 614 (1986).
13. D. Gabor, *Proc. R. Soc. London Ser. A* **197**, 454 (1949).
14. J. P. Woerdman, *Opt. Commun.* **2**, 212 (1971).
15. H. J. Eichler, *Habilitationsschrift* (Technische Universität, Berlin, 1970).
16. K. Duppen, D. P. Weitekamp, D. A. Wiersma, *Chem. Phys. Lett.* **106**, 147 (1984).
17. C. K. Shan and S. O. Sari, *Appl. Phys. Lett.* **56**, 403 (1974).
18. J. M. Clemens, J. Najbar, I. Bronstein-Bonte, R. M. Hochstrasser, *Opt. Commun.* **47**, 271 (1983).
19. J. D. Kafka, B. H. Kolner, T. Baer, D. M. Bloom, *Opt. Lett.* **9**, 505 (1984).
20. A. M. Johnson and W. M. Simpson, *J. Opt. Soc. Am. B* **2**, 619 (1985); *IEEE J. Quantum Electron.* **22**, 133 (1986).
21. W. H. Knox, M. C. Downer, R. L. Fork, C. V. Shank, *Opt. Lett.* **9**, 552 (1984).
22. I. N. Duling, T. Norris, T. Sizer II, P. Bado, G. A. Mourou, *J. Opt. Soc. Am. B* **2**, 615 (1985).
23. W. H. Hesselink and D. A. Wiersma, *Chem. Phys. Lett.* **56**, 227 (1978).
24. R. S. Longhurst, *Geometrical and Physical Optics* (Wiley, New York, ed. 2, 1967).
25. K. A. Nelson, R. Casalegno, R. J. Dwayne Miller, M. D. Fayer, *J. Chem. Phys.* **77**, 1144 (1982).
26. D. P. Weitekamp, K. Duppen, D. A. Wiersma, *Chem. Phys. Lett.* **102**, 139 (1983).
27. W. H. Hesselink and D. A. Wiersma, *J. Chem. Phys.* **73**, 648 (1980).
28. K. Duppen, D. P. Weitekamp, D. A. Wiersma, *ibid.* **79**, 5835 (1983).
29. J. R. Salcedo, A. E. Siegman, D. D. Dlott, M. D. Fayer, *Phys. Rev. Lett.* **41**, 131 (1978).
30. Y. Aoyagi, Y. Segawa, S. Namba, *Phys. Rev. B* **25**, 1453 (1982).
31. T. S. Rose, R. Righini, M. D. Fayer, *Chem. Phys. Lett.* **106**, 13 (1984).
32. A. L. Smirl, T. F. Boggess, B. S. Wherrett, G. P. Perryman, A. Miller, *IEEE J. Quantum Electron.* **19**, 690 (1983).
33. G. Eyring and M. D. Fayer, *J. Chem. Phys.* **81**, 4314 (1984).
34. A. L. Smirl, T. F. Boggess, B. S. Wherrett, G. P. Perryman, A. Miller, *Phys. Rev. Lett.* **49**, 933 (1982).
35. J. B. W. Morsink, W. H. Hesselink, D. A. Wiersma, *Chem. Phys. Lett.* **64**, 1 (1979).
36. J. B. W. Morsink and D. A. Wiersma, in *Laser Spectroscopy*, H. Walther and K. W. Rothe, Eds. (Springer Series in Optical Sciences, New York, 1979), p. 404.
37. T. W. Mossberg, *Laser Focus* **22**, 36 (September 1986).
38. K. Duppen, D. P. Weitekamp, D. A. Wiersma, *Chem. Phys. Lett.* **108**, 551 (1984).
39. N. Morita and T. Yajima, *Phys. Rev. A* **30**, 2525 (1984); S. Asaka, H. Nakatsuka, M. Fujiwara, M. Matsuoka, *ibid.* **29**, 2286 (1984); T. Hattori, A. Terasaki, T. Kobayashi, *ibid.* **35**, 715 (1987).
40. J. W. Goodman, *Statistical Optics* (Wiley, New York, 1985).

The Nerve Growth Factor 35 Years Later

RITA LEVI-MONTALCINI

Embryogenesis is in some way a model system. It has always been distinguished by the exactitude, even punctilio, of its anatomical descriptions. An experiment by one of the great masters of embryology could be made the text of a discourse on scientific method. But something is wrong, or has been wrong. There is no theory of development in the sense in which Mendelism is a theory that accounts for the results of breeding experiments. There has therefore been little sense of progression or timeliness about embryological research. Of many papers delivered at embryological meetings, however good they may be in themselves, one too often feels that they might have been delivered 5 years beforehand without making anyone much the wiser, or deferred for 5 years without making anyone conscious of a great loss.—P. MEDAWAR

THIS FEELING OF FRUSTRATION SO INCISIVELY CONVEYED by these considerations by P. Medawar (*1*), in the passage quoted above, pervaded, in the forties, the field of experimental embryology, which had been enthusiastically acclaimed in the mid-thirties when the upper lip of the amphibian blastopore brought this area of research to the forefront of the biological stage. The side branch of experimental neuroembryology, which had stemmed from the common tree and was entirely devoted to the study of the trophic interrelations between neuronal cell populations, and between these and the innervated organs and tissues, was then in its initial vigorous growth phase. It, in turn, suffered from a sharp decrease in the enthusiasm that had inflamed the pioneers in this field, ever since R. G. Harrison delivered his celebrated lecture on this topic at the Royal Society in London in 1935 (*2*). Although the alternate "wax and wane" cycles are the rule rather than the exception in all fields of human endeavor, in that of biological sciences the "wane" is all too often indicative of a justified loss of faith in the rational and methodical approach that had at first raised so much hope.

A brief account of the state of the art of experimental neuroembryology in the forties, when interest in this approach to the study of the developing nervous system was waning, is a prerequisite for understanding the sudden unforeseeable turn of events which resulted in the discovery of the nerve growth factor.

Experimental Neuroembryology in the Early Forties

The replacement, in 1934 by Viktor Hamburger, of the chick embryo for the amphibian larva as object of choice for the analysis of the effects of limb bud extirpation on spinal motor neurons and sensory nerve cells innervating the limbs (*3*) signaled the beginning of a long series of investigations centered on the analysis of this and related experimental systems in avian embryos. Here I shall list only the major advantages offered by the chick embryo over amphibian larvae as objects of neurological investigations.

The author is a professor at the Institute of Cell Biology, National Research Council, Rome, Italy. This article is the lecture she delivered in Stockholm, Sweden, 8 December 1986, when she received the Nobel Prize in Physiology or Medicine, which she shared with Stanley Cohen. It is published here with the permission of the Nobel Foundation and will also be included in the complete volume of *Les Prix Nobel en 1986* as well as in the series *Nobel Lectures* (in English) published by Elsevier Publishing Company, Amsterdam and New York. The lecture by Dr. Cohen will appear in a later issue.